Supporting Information

Transparent CdS@TiO_2 Nanotextile Photoanode with Boosted Photoelectrocatalytic Efficiency and Stability

Long Liu,[a,b] HuilinHou,[a] Lin Wang,[a] RuiXu,[b] YongLei,[b] ShaohuaShen,[c] Dongjiang Yang[d,e,*] and Weiyou Yang[a,*]

[a] Institute of Materials, Ningbo University of Technology, Ningbo 315016, P.R. China.

[b] Institut für Physik & IMN MacroNano (ZIK), Technische Universität Ilmenau, Ilmenau 98693, Germany.

[c] International Research Center for Renewable Energy, State Key Laboratory of Multiphase Flow in Power Engineering, Xi'an Jiaotong University, Shanxi 710049, P.R. China.

[d] Collaborative Innovation Center for Marine Biomass Fibers Materials and Textiles of Shandong Province School of Environmental Science and Engineering, Qingdao University, Qingdao 266071, P. R. China.

[e] Queensland Micro- and Nanotechnology Centre (QMNC), Griffith University, Nathan, Brisbane, QLD 4111, Australia.

Corresponding Authors: E-mails: d.yang@qdu.edu.cn (D. Yang) and weiyouyang@tsinghua.org.cn (W. Yang)

This supplementary file includes:

Supplementary Notes

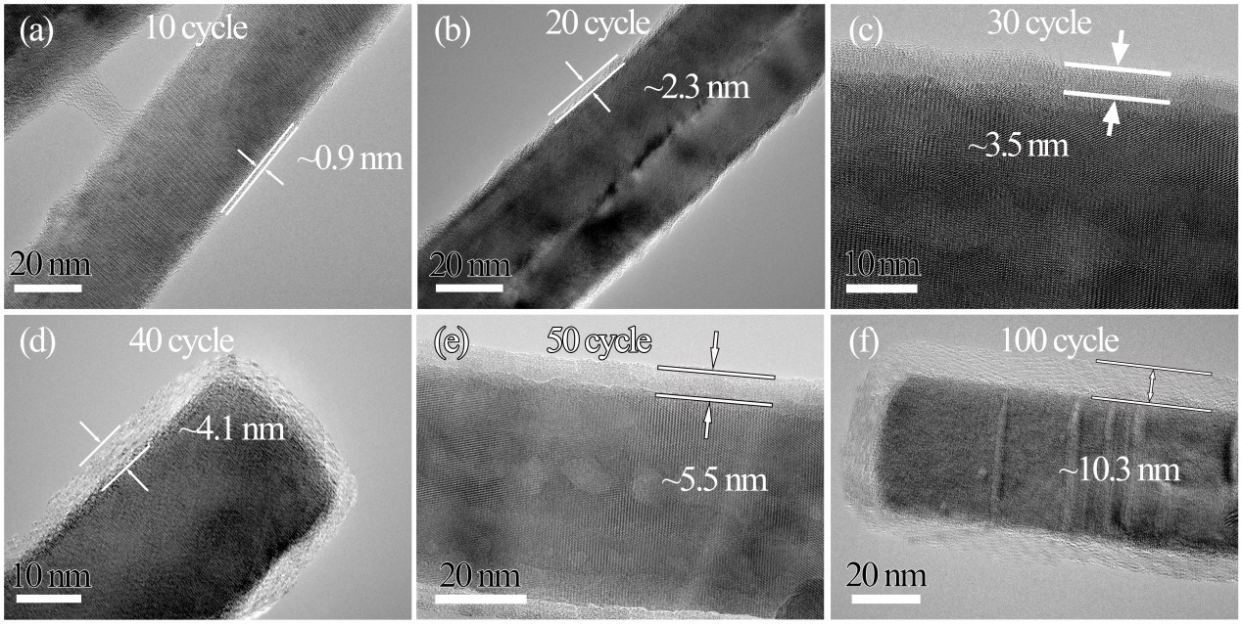

Fig. S1. Typical TEM images of the as-grown CdS@TiO_2 nanowires with various ALD cycles.

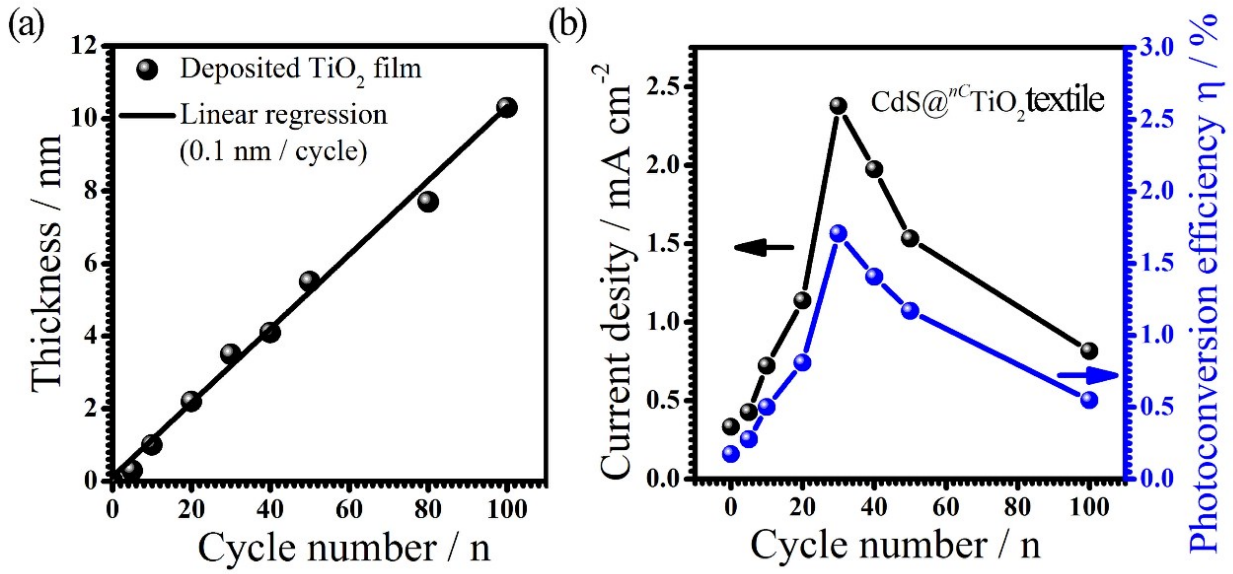

Fig. S2. (a) The relationship between the shell thicknesses *vs.* ALD cycles. (b) The relationship of current densities and photoconversion efficiencies *vs.* ALD cycles (b).

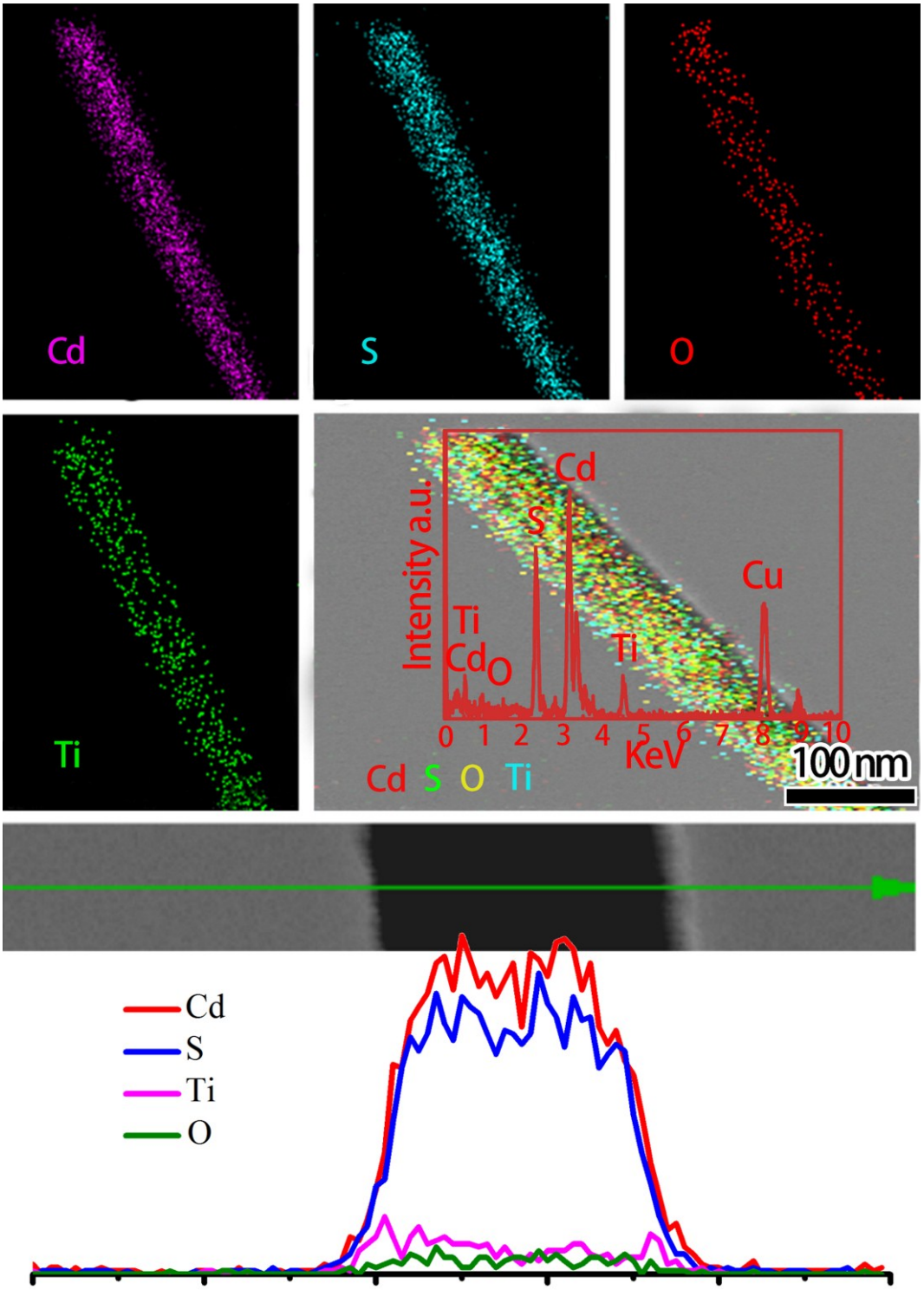

Fig. S3. The representative element mappings recorded from a single CdS@TiO_2 core/shell nanowire.

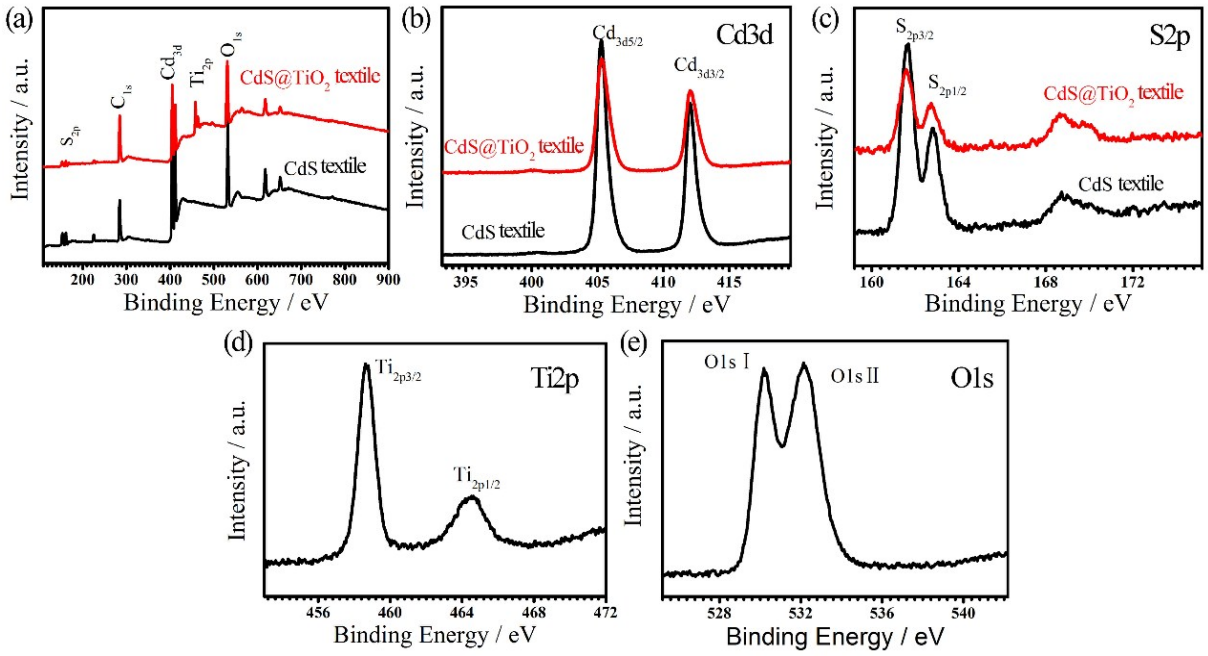

Fig. S4. (a) Typical XPS survey scans of CdS and CdS@TiO_2 textile films, (b-c) the Cd 3d and S 2p core level spectra of the CdS and CdS@TiO_2 textile films, respectively. (d-e) the Ti 2p and O 1s core level spectra, respectively.

Fig. S4a gives the general XPS scan spectrum of CdS and CdS@$^{30C}TiO_2$ textile films. As shown in Fig. 4b, the Cd 3d core level XPS spectrum has two peaks at 404.8 eV ($3d_{5/2}$) and 411.6 eV ($3d_{3/2}$). The S 2p core level spectrum indicates that there are two chemically distinct species in the spectrum. The peak at 161.9 eV is assigned to the sulfide and the peak at 168.4 eV is assigned to sulfur in sulfate (Fig. S4c). The reduced peak intensities of Cd and S within the CdS@TiO_2 counterpart indicate the existence of TiO_2 protection film. The two symmetric peaks of Ti 2p located at 458.6 and 464.4 eV are ascribed to the Ti 2p3/2 and Ti 2p1/2 for the TiO_2 sample, respectively, which indicate a formal valence of four (Ti^{4+}, Fig. S4d).The O1s peak at 530.1 eV (OI) is attributed to the Ti-O bond of TiO_2, and the one at 532.1 eV (OII) responds to the OH group on the surface, respectively (Fig. S4e).

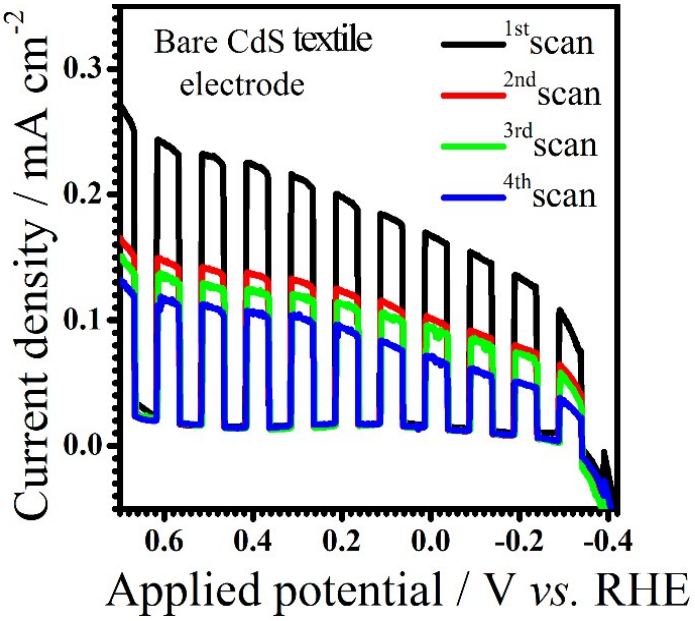

Fig. S5. Photoelectrocatalytic *J-V* curves of pristine CdS textile electrode as a function of the scan times.

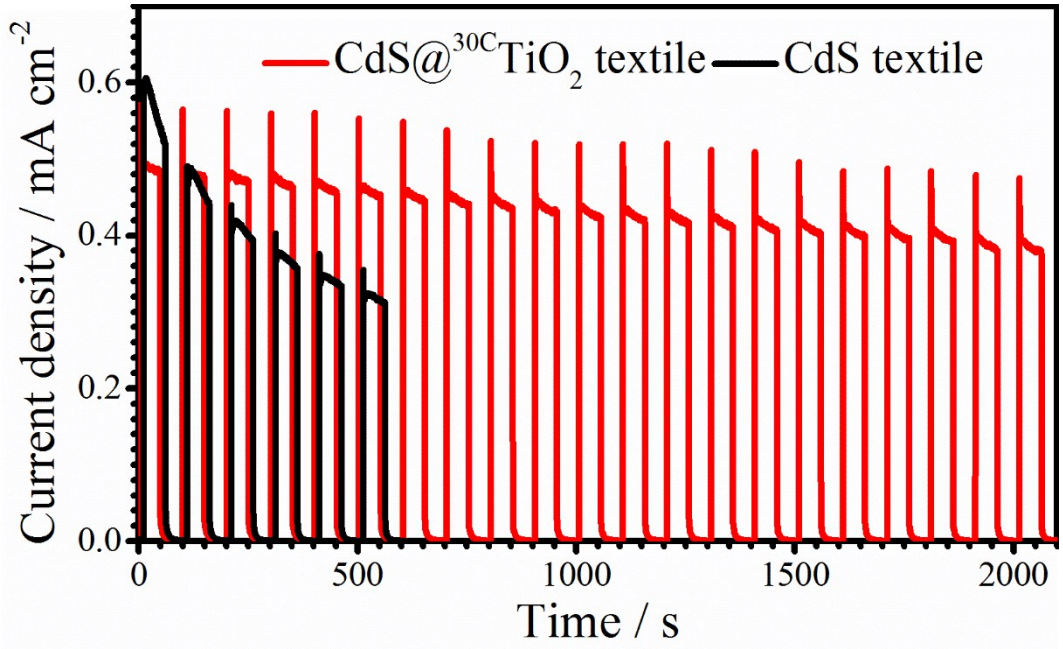

Fig. S6. Photocurrent response in Na_2SO_4 aqueous solution (0.5 M, pH = 6.8) of CdS@$^{30C}TiO_2$ and CdS textile electrode under simulated sunlight at 0.1 V (*vs.* Ag/AgCl) with intermittent illumination.

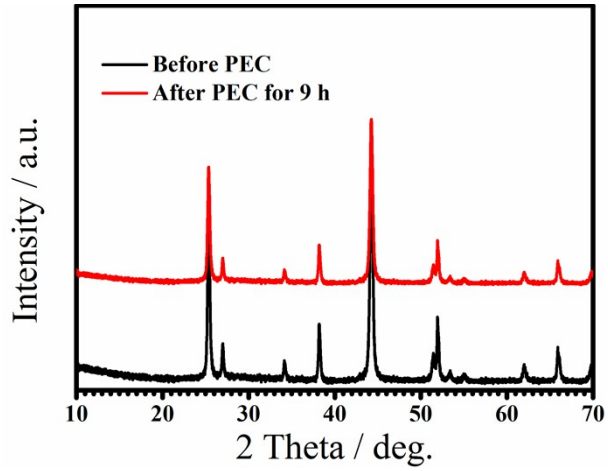

Fig. S7. Typical XRD patterns of CdS@^{30C}TiO$_2$ nanotextile photoanode before and after PEC.

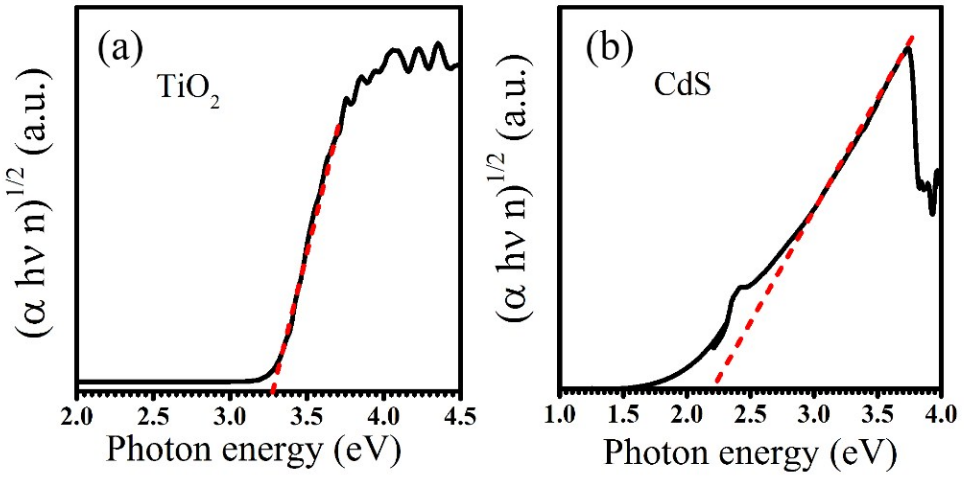

Fig. S8. (a) and (b) The Tauc plots of ALD-grown TiO_2 layer and CdS textile film, respectively.

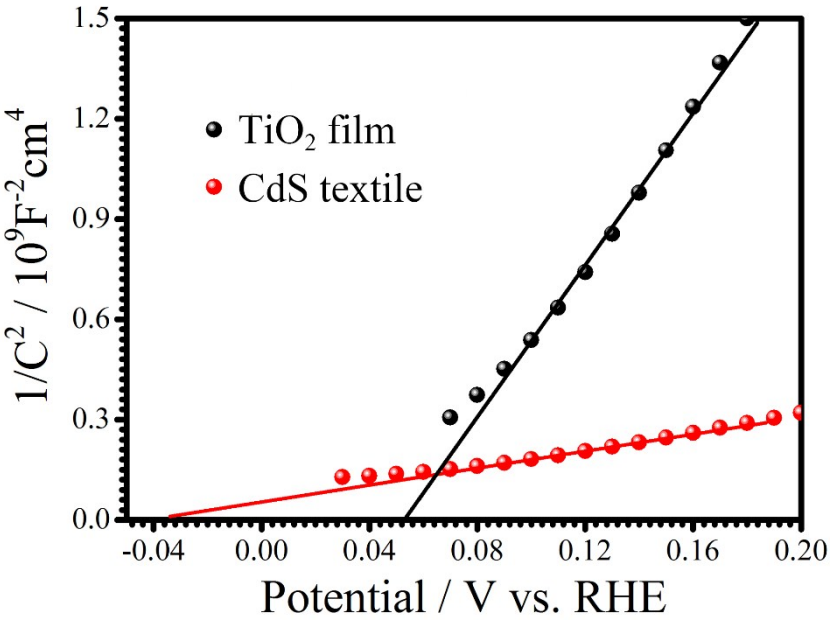

Fig. S9. The Mott–Schottky plots of the photoanodes based on TiO_2 film and CdS textile.

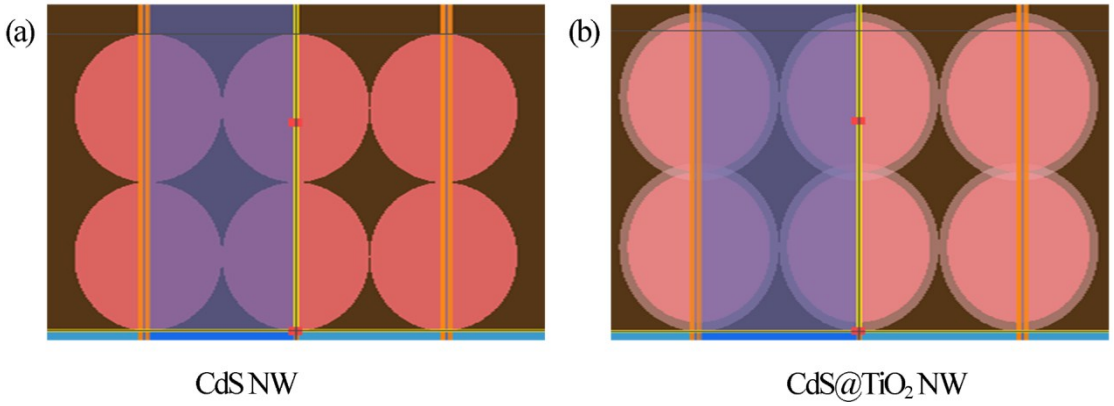

Fig. S10. (a) and (b) The cross-section models of CdS andCdS@TiO_2 NWs, respectively.

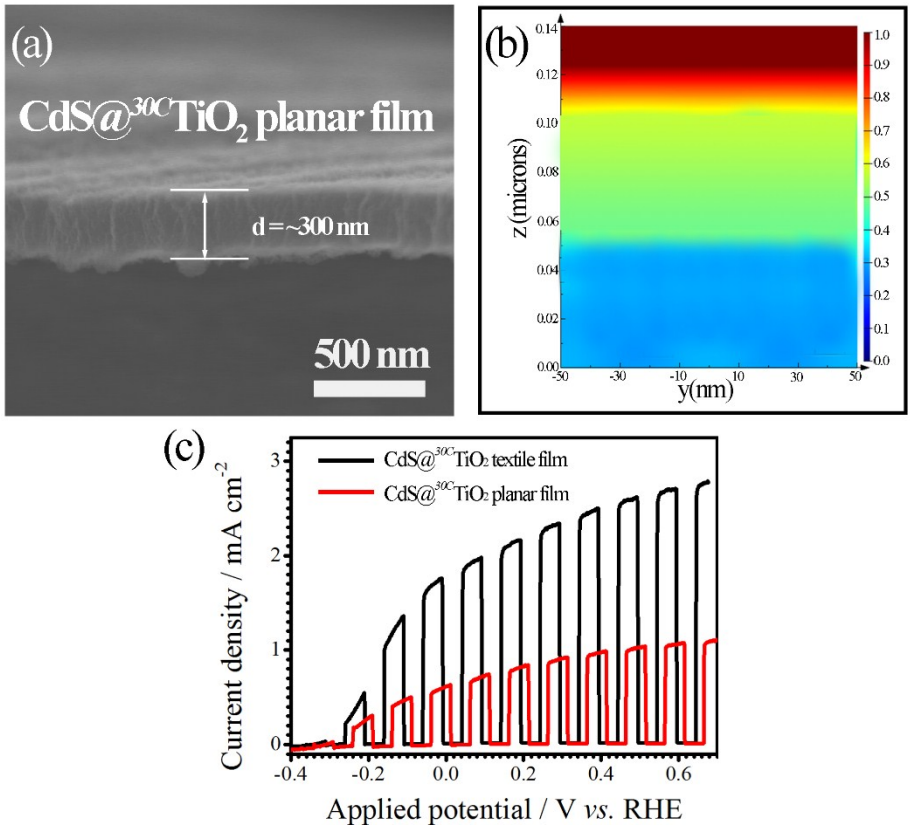

Fig. S11. (a) SEM image of electro-deposition of CdS flat film with 30 cycle TiO_2 deposition. (b) The simulated cross-sectional electromagnetic wave distributions of CdS@^{30C}TiO planar film at the wavelength of 300 nm. (c) The PEC response of planar and textile film. The CdS planar film was cathodically deposited from an aqueous solution of 0.2 M $CdCl_2$• $2H_2O$ and 0.01 M of $Na_2S_2O_3$ with a pH value of 2.5.

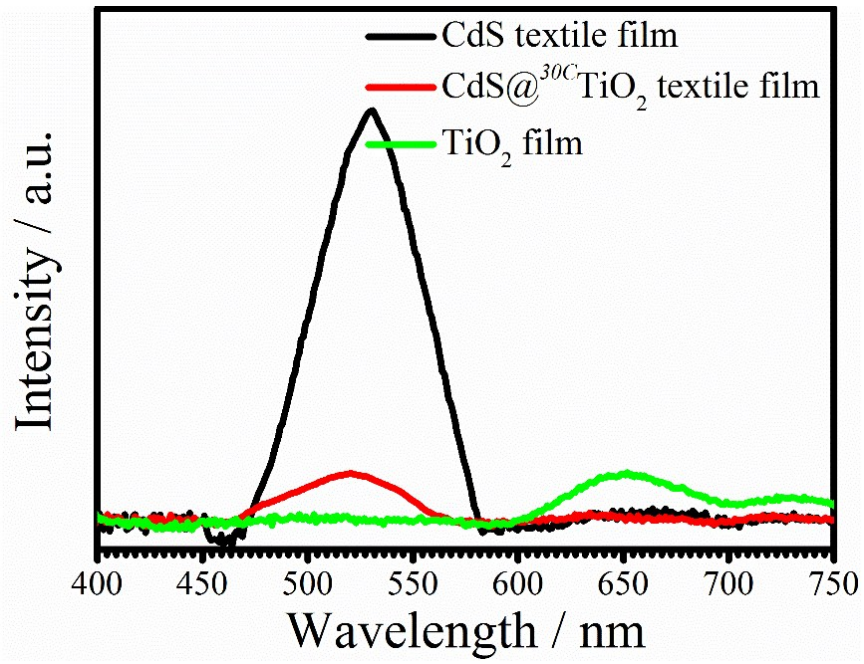

Fig. S12. Typical PL spectra of CdS, CdS@$^{30C}TiO_2$ and TiO_2 films. It seems thatthe CdS@$^{30C}TiO_2$ NWs exhibit a much weaker peak from 480 to 580 nm than CdS NWs under excitation at 325 nm, indicating the effective charge transfer between CdS and TiO_2, which can be ascribed to the lower recombination probability of photoinduced electrons and holes. The transfer of electrons from CdS to TiO_2 facilitates the separation of photoinduced electrons and holes in TiO_2, and thus inhibits the recombination of the photogenerated charge carriers.

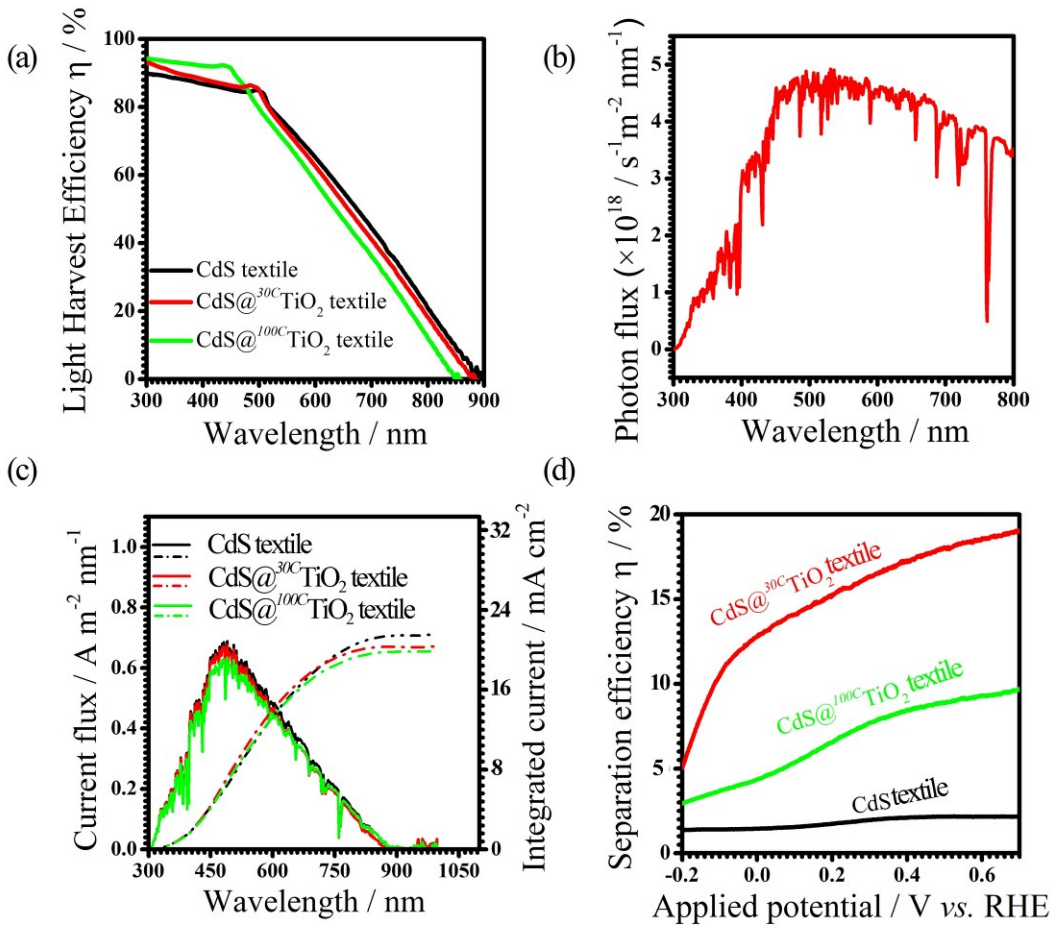

Fig. S13. (a) The light harvesting efficiencies of the CdS, CdS@^{30C}TiO$_2$ and CdS@^{100C}TiO$_2$ nanotextile photoanodes. (b) The AM 1.5 photon flux incident at each wavelength. (c) The current flux $J_{flux}(\lambda)$ and the integrated current $J_{abs}(\lambda)$ of these samples. (d) The charge separation efficiencies of these three samples.

Table S1. Summary of typical PEC performances of 1D CdS nanostructures recently reported in the literatures.

Photocatalyst	Catalyst amount /mg	Scavenger	Light source	Photocurrent at 0 V vs. RHE (mA/cm^2)	Amount of H_2 evolution (mmol/g/h)	Ref.
CdS@TiO_2	**0.62**	**Na_2S + Na_2SO_3**	**Simulated sunlight**	**1.8**	**47.5**	**This work**
CdS/WS_2	200	Lactic acid	300 W Xe lamp ($\lambda \geq 400$ nm)	-	27.5	1
CdS/WS_2-MoS_2	1	Lactic acid	Simulated sunlight	1.0×10^{-3}	209	2
CdS/WS2-graphene	8	Na_2S + Na_2SO_3	350 W Xe lamp ($\lambda \geq 420$ nm)	-	1.842	3
MoS_2/CdS	200	Lactic acid	300 W Xe lamp ($\lambda \geq 400$ nm)	1.6 (0 V *vs.* Ag/AgCl)	58.3	4
MoS_2/CdS	1	Na_2S + Na_2SO_3	Simulated sunlight	1.6 (0 V *vs* SCE)	35	5
MoS_2/CdS	20	Lactic acid	Simulated sunlight	-	174	6
CuO/CdS/TiO_2 (with Pt)	-	K_2HPO_4/K H_2PO_4	Simulated sunlight	-1.4	0.4 (μmol/h)	7
CdS/TiO_2	2	Na_2SO_4	300W xenon lamp	0.12	-	8
5% Pt/CdS-N	50	lactic acid	300 W Xe lamp($\lambda \geq 400$ nm)	0.015	16.27	9
CdS-Co_3O_4	50	Na_2S + Na_2SO_3	300 W Xe lamp($\lambda \geq 420$ nm)	-	0.23	10
$Co(OH)_2$/CdS	200	Na_2SO_4	LED (3 W, 365 nm)	0.027	14.43	11
MoS_2/CdS	-	lactic acid	300 W Xe lamp ($\lambda \geq 400$ nm)	4×10^{-3}	1800 (μmol/h)	12
Ni_2P/CdS	1	Na_2S + Na_2SO_3	300 W Xe lamp ($\lambda \geq 400$ nm)	-	553	13
CdS/ZnS-0.5	-	Na_2S + Na_2SO_3	300 W Xe lamp ($\lambda \geq 420$ nm)	0.01	240 (μmol/h)	14
CdS-$BiVO_4$	6	Ammonium oxalate	300 W Xe lamp ($\lambda \geq 420$ nm)	5×10^{-3}	-	15
CdS NRPJs	20	Na_2S + Na_2SO_3	300 W Xe lamp ($\lambda \geq 420$ nm)	0.05	26	16
$Ni(OH)_2$-CdS/g-C_3N_4	1	Na_2S + Na_2SO_3	300 W Xe lamp ($\lambda \geq 420$ nm)	0.03	115.18	17
CdS/$ZnIn_2S_4$	0.1	Na_2S + Na_2SO_3	300 W Xe lamp ($\lambda \geq 420$ nm)	6	-	18

Notes S1. Calulations of applied bias photon-to-current efficiency (ABPE)

The ABPE was calculated as follows:

ABPE(%)= ((total power output−electrical power output)/light power input)×100

$$= \mathrm{j}_p((E^0_{rev} - \left|E_{app}\right|) / I_0\right|) \times 100$$

Where j_p is the photocurrent density, $j_p E^0_{rev}$ is the total power output, $j_p|E_{app}|$ is the electrical power input, I_0 is the power density of incident light. E^0_{rev} is the standard reversible potential, which is 1.23 V *vs.* RHE. The applied potential of $E_{app}=E_{meas}-E_{aoc}$, where E_{meas} is the electrode potential (*vs.* RHE) of the working electrode at which the photocurrent was measured under illumination, and E_{aoc} is the electrode potential (*vs.* RHE) of the same working electrode at open circuit conditions under the same illumination and electrolyte.

Notes S2. Calculation on the carrier density from Mott–Schottky plots.

Mott−Schottky analysis is based on the assumption, that the capacitance of the space charge layer is much less than that of the Helmholtz layer. Mott−Schottky plots were conducted and shown in Fig. S6. Mott−Schottky relationships of *n*- and *p*-type semiconductors are expressed as:

$$\frac{1}{C^2} = \frac{2}{\varepsilon\varepsilon_0 e N_d A^2}[(E - E_{FB}) - \frac{kT}{e}]$$

Where ε_0 is the permittivity of vacuum (8.854×10^{-12} F/m), ε is the dielectric constant of TiO_2 (*i.e.,* 170) and CdS (*i.e.,* 8.7), and e is the electronic charge (*i.e.,* 1.603×10^{-19} C). N_d refers the donor densities, which is calculated from the slopes of the curves. T is the operation temperature (*i.e.,* 298 K), and k is the Boltzmann's constant (*i.e.,*1.38×10^{-23} J/K). E is the electrode potential, and E_{FB} is the flat-band potential, and C is the depletion-layer capacitance. The carried densities of CdS and TiO_2 calculated by the fitting curves are 1.14×10^{21} and 6.83×10^{18} cm^{-3}, respectively. The low carrier density of TiO_2 layer represents its poor conductivity, which is why the thicker TiO_2 film is seldom used as the cocatalyst.

Notes S3. Calculation of separation and injection efficiency

The photocurrent is determined by:

$$J_{H_2O} = J_{abs} \cdot \eta_{sep} \cdot \eta_{transfer}$$

Where J_{H2O} is the H_2O oxidation photocurrent, J_{abs} is the photon absorption rate (namely the photocurrent density), η_{sep} is the charge separation efficiency, $\eta_{transfer}$ is the rate of charge injection.

Here, the rate of charge transfer to the electrolyte by oxidation of sacrificial agents at the semiconductor/electrolyte interface is very fast. Accordingly, it can be assumed that the surface recombination of the charges is eliminated (*i.e.,* $\eta_{transfer}\approx 100\%$). That is to say,

$$J_{Na_2SO_3} = J_{abs} \cdot \eta_{sep}$$

The $J_{abs}(\lambda)$ can be calculated by integrating the current flux $J_{flux}(\lambda)$ to wavelength λ:

$$J_{abs}(\lambda) = \int J_{flux}(\lambda) d\lambda$$

$$J_{flux}(\lambda) = N_{ph}(\lambda) \cdot LHE(\lambda) \cdot e$$

Where λ is the bandedge of the semiconductor absorption, $J_{flux}(\lambda)$ is the current flux at λ, $N_{ph}(\lambda)$ is thephoton flux, e is the elementary charge (*i.e.,*1.602×10^{-19}), $LHE(\lambda)$ is the light harvest efficiency which can be gotten from the absorption $A(\lambda)$:

$$LHE(\lambda) = 1 - 10^{-A(\lambda)}$$

References

1. X. Hai, K. Chang, H. Pang, M. Li, P. Li, H. Liu, L. Shi and J. Ye, *J. Am. Chem. Soc.*, 2016, **138**, 14962-14969.
2. D. A. Reddy, H. Park, R. Ma, D. P. Kumar, M. Lim and T. K. Kim, *ChemSusChem*,

2017, **10**, 1563–1570.

3. Q. Xiang, F. Cheng and D. Lang, *ChemSusChem*, 2016, **9**, 996-1002.

4. X.L. Yin, G.Y. He, B. Sun, W.-J. Jiang, D.J. Xue, A.-D. Xia, L.J. Wan and J.S. Hu, *Nano Energy*, 2016, **28**, 319-329.

5. A. Pareek, H. G. Kim, P. Paik and P. H. Borse, *J. Mater. Chem. A*, 2017, **5**, 1541-1547.

6. D. P. Kumar, S. Hong, D. A. Reddy and T. K. Kim, *J. Mater. Chem. A*, 2016, **4**, 18551-18558.

7. W. Septina, R. R. Prabhakar, R. Wick, T. Moehl and S. D. Tilley, *Chem. Mater.*, 2017, **29**, 1735–1743.

8. P. Zhou, Z. Le, Y. Xie, J. Fang and J. Xu, *J. Alloys Compd.*, 2017, **692**, 170-177.

9. L. Zhang, X. Fu, S. Meng, X. Jiang, J. Wang and S. Chen, *J. Mater. Chem. A*, 2015, **3**, 23732-23742.

10. J. Yuan, J. Wen, Q. Gao, S. Chen, J. Li, X. Li and Y. Fang, *Dalton Trans.*, 2015, **44**, 1680-1689.

11. X. Zhou, J. Jin, X. Zhu, J. Huang, J. Yu, W.Y. Wong and W.-K. Wong, *J. Mater. Chem. A*, 2016, **4**, 5282-5287.

12. J. He, L. Chen, F. Wang, Y. Liu, P. Chen, C. T. Au and S. F. Yin, *ChemSusChem*, 2016, **9**, 624-630.

13. Z. Sun, H. Zheng, J. Li and P. Du, *Energy Environ. Sci.*, 2015, **8**, 2668-2676.

14. D. Jiang, Z. Sun, H. Jia, D. Lu and P. Du, *J. Mater. Chem. A*, 2016, **4**, 675-683.

15. B. Han, S. Liu, Y.J. Xu and Z.-R. Tang, *RSC Adv.*, 2015, **5**, 16476-16483.

16. K. Li, M. Han, R. Chen, S. L. Li, S. L. Xie, C. Mao, X. Bu, X. L. Cao, L. Z. Dong and P. Feng, *Adv. Mater.*, 2016, **28**, 8906-8911.

17. Z. Yan, Z. Sun, X. Liu, H. Jia and P. Du, *Nanoscale*, 2016, **8**, 4748-4756.

18. B. Xu, P. He, H. Liu, P. Wang, G. Zhou and X. Wang, *Angew. Chem. Int. Ed.*, 2014, **53**, 2339-2343.